DUAL COMPUTATIONS OF NON-ABELIAN YANG-MILLS ON THE LATTICE

J. WADE CHERRINGTON[1], J. DANIEL CHRISTENSEN[2], AND IGOR KHAVKINE[3]

[1,3]Department of Applied Mathematics, University of Western Ontario, London, Ontario, Canada
[2]Department of Mathematics, University of Western Ontario, London, Ontario, Canada
E-mail: jcherrin@uwo.ca, jdc@uwo.ca, and ikhavkin@uwo.ca

ABSTRACT. In the past several decades there have been a number of proposals for computing with dual forms of non-abelian Yang-Mills theories on the lattice. Motivated by the gauge-invariant, geometric picture offered by dual models and successful applications of duality in the $U(1)$ case, we revisit the question of whether it is practical to perform numerical computation using non-abelian dual models. Specifically, we consider three-dimensional $SU(2)$ pure Yang-Mills as an accessible yet non-trivial case in which the gauge group is non-abelian. Using methods developed recently in the context of spin foam quantum gravity, we derive an algorithm for efficiently computing the dual amplitude and describe Metropolis moves for sampling the dual ensemble. We relate our algorithms to prior work in non-abelian dual computations of Hari Dass and his collaborators, addressing several problems that have been left open. We report results of spin expectation value computations over a range of lattice sizes and couplings that are in agreement with our conventional lattice computations. We conclude with an outlook on further development of dual methods and their application to problems of current interest.

1. INTRODUCTION

In this work we describe recent progress in lattice gauge theory (LGT) computations in a model dual to pure Yang-Mills theory. The dual model we consider is based upon the character expansion of the amplitude at each fundamental plaquette, a procedure that has been known since the early days of lattice gauge theory [25, 36, 42]. To date, the most common use of this duality transformation has been in the strong-coupling expansion, as described for example in [22, 26, 32] and references therein. Because of this historical association with strong-coupling approximations, we should emphasize here that it is the exact dual model that we compute with, sampling from the full space of dual configurations to find the expectation values of observables. The first steps towards such dual computations in the non-abelian case were taken by Hari Dass et al. in [16, 17, 20]; more recently, interest in dual computations of lattice Yang-Mills theory has grown within the spin foam community [10, 33, 39].

Perhaps the most significant change in passing to the dual model is that the variables include discrete labels assigned to lattice plaquettes. This aspect alone gives a very different character to the computation when compared to the conventional formulation of LGT, where continuous group-valued variables are assigned to lattice edges. Another significant difference is the fact that the discrete labels must satisfy certain constraints, making the choice of Metropolis moves non-trivial (see Section 2). The allowed configurations can be viewed as closed, branched surfaces colored by the irreducible representations of the gauge group. To illustrate, some renderings of non-zero dual configurations are shown in Figure 1.

As general motivation for the dual approach, we observe that the dual configurations have a gauge-independent meaning rooted in the statistical geometry of the two-dimensional branched surfaces, providing a compelling geometric picture for the evolution of the physical degrees of freedom. For example, in the strong-coupling limit, the dual picture provides a straightforward analytic proof of confinement (see, e.g., [32] and references therein). By making topological excitations manifest, a dual model is well suited to evaluating proposed mechanisms of quark confinement, such as the dual superconductor picture. This advantage has already been demonstrated in the abelian $U(1)$ case [23, 37, 38, 40, 44, 45, 46] and has also been remarked upon in the non-abelian case [33]. Recently, effective theories have been derived directly from the dual theory [11], and so we believe a computational framework for numerical computations within the dual theory is timely.

1

While results have been reported with dual models in the $U(1)$ theory, the non-abelian case has presented a greater computational challenge. As a testing ground for dual non-abelian simulation algorithms, we focus in the present work on $SU(2)$ pure Yang-Mills in three space-time dimensions. The observable we study is the average spin (see Section 3) which is convenient for testing as it takes a simple form on both sides of the duality. In describing our algorithm and results, we address potential problems for non-abelian dual computations that were discussed in the work of Hari Dass et al. [17, 20], the most critical of which were the construction of ergodic moves and a sign problem. The results obtained with our Metropolis algorithm appear to overcome these difficulties for the range of lattice sizes and coupling constants presented here. With the current algorithm, a difficulty (discussed in Section 4.2) emerges at weak coupling, however our expectation is that it will be resolved with a more refined form of the algorithm.

Although there is an intriguing possibility that dual algorithms may eventually outperform their conventional equivalents in certain contexts, the present work focuses on the general features of computing with dual algorithms and verifying their correctness against a conventional lattice code. In future work, we will address more optimized implementations of the algorithms described here, with the ultimate goal of providing results in four dimensions with lattice sizes typical of contemporary lattice QCD. An important next step will be to extend our methods to Wilson loop observables crucial to the study of quark confinement and glueball spectra; this work is currently in progress [7].

The paper is organized as follows. In Section 2, we define the dual model under study and describe a Metropolis algorithm for numerical computations. In Section 3, we describe computations on a 2^3 lattice that allow us to verify threefold agreement (within statistical error) between dual Metropolis, conventional Metropolis and the exact partition function. In Section 4, we describe our computations for lattice sizes of 4^3, 8^3, and 16^3 and report agreement between dual and conventional Metropolis results, again within statistical error. Section 5 provides a brief outlook on generalizing the algorithm and Section 6 presents our conclusions. Some details relevant for performing the computations are given in the Appendix, which also shows how the dual amplitude formula used by Hari Dass [17, 20], originally given in [3] and discussed in [13, 14], fits into the spin foam formalism used to develop our algorithm.
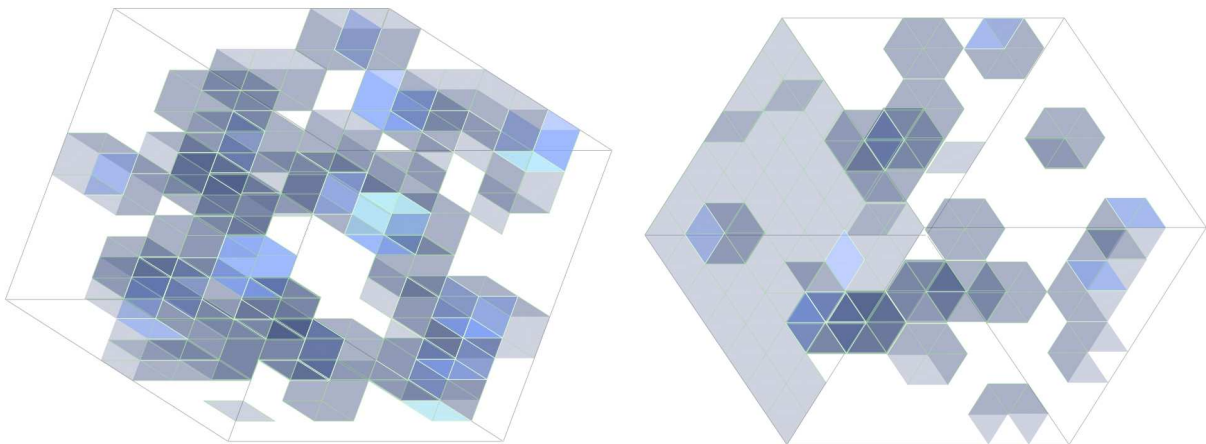

FIGURE 1. Two examples of dual configurations on a 6^3 lattice. Opposite sides of the lattice are identified. In the right-hand figure a sheet of flux spanning the lattice is present, allowed due to the non-trivial homology of the 3-torus. In the left-hand figure there are no such sheets present.

2. Review of The Dual Model And Algorithm Construction

In this section we define the dual model for $SU(2)$ pure Yang-Mills on a hyper-cubic lattice and describe a Metropolis algorithm for performing dual computations. Of particular relevance to our present work is the application of diagrammatic methods and spin foam formalism, as described for

example in [10, 33, 34], a critical feature being the expression of group integrals of representation matrices and their contractions as sums over intertwiners[1]. While the spin foam formalism for dual models is a more recent development, the construction of exact dual non-abelian models has a longer history [1, 2, 3, 14, 15, 18, 19]. Traditional derivations of the duality transformation and their use in strong-coupling expansions can be found in the texts [22, 32].

2.1. **Review of pure Yang-Mills theory on the lattice.** First we recall the Euclidean partition function of pure Yang-Mills theory in D dimensions, with gauge group $G = SU(N)$, where $N \geq 2$ (we shall later specialize to the $SU(2)$ case). It takes the form

$$\mathcal{Z} = \int \mathcal{D}A \, \exp(-S), \tag{1}$$

with A_μ^a the gauge field, S the action functional, and $\mathcal{D}A$ the functional integration measure. In the continuum version of the theory the standard action functional is

$$S \equiv S[A] = \frac{1}{4g^2} \int d^D x \, F_{\mu\nu}^a F_a^{\mu\nu}, \tag{2}$$

where $F_{\mu\nu}^a$ is the field strength tensor and g the continuum coupling. Unfortunately, the continuum functional measure $\mathcal{D}A$ is not well-defined.

One way to give the above path integral rigorous meaning and, at the same time, make it amenable to computational treatment, is to put the theory on a discrete finite lattice. The simplest variant uses a hyper-cubic lattice. Let E and P denote respectively the sets of edges and plaquettes of a hyper-cubic lattice in D dimensions. The gauge field A is replaced by gauge group elements g_e assigned to each oriented lattice edge $e \in E$. The same edge with opposite orientation gets g_e^{-1} instead of g_e. The functional integral measure can now be replaced by an integral over the product of $|E|$ copies of G using Haar measure:

$$\mathcal{D}A \equiv \prod_{e \in E} dg_e. \tag{3}$$

At the same time, the action functional is replaced by a discretized version, $S \equiv S[g]$, that must reproduce the continuum action $S[A]$ as the lattice spacing is taken to zero. The discretized action is usually split into a sum over plaquettes, $S[g] = \sum_{p \in P} S(g_p)$, where the group element g_p is the holonomy around an oriented plaquette p. That is, $g_p = g_1 g_2 g_3 g_4$, where g_i is either the group element assigned to the ith edge of p or its inverse if the orientations of p and the ith edge are opposing. This yields the conventional lattice partition function

$$\mathcal{Z} = \int \prod_{e \in E} dg_e \, e^{-\sum_{p \in P} S(g_p)}. \tag{4}$$

There are many candidate discretized plaquette actions $S(g_p)$. While the Wilson action [43] is perhaps the most well-known in conventional LGT (it was also used in the dual computations of [16, 17, 20]), a variety of actions $S(g_p)$ leading to the correct continuum limit are known and have been used in the literature [21, 28, 29]. In the present work, we use the *heat kernel action* [30]; in the dual model this action leads to plaquette factors that are particularly easy to compute. The heat kernel action (at lattice coupling γ) for a fundamental plaquette p and plaquette holonomy g_p is

$$e^{-S(g_p)} = \frac{K(g_p, \frac{\gamma^2}{2})}{K(I, \frac{\gamma^2}{2})}, \tag{5}$$

where the heat kernel K, which is a function of a group element g and of a "time" parameter t, satisfies a diffusion type differential equation

$$\frac{\partial}{\partial t} K(g, t) = \Delta K(g, t), \quad K(g, 0) = \delta_I(g). \tag{6}$$

Here Δ is the Laplace-Beltrami operator on G and δ_I is the delta function at the group identity I. The denominator in (5) represents a normalization of the partition function in which flat holonomies

---

[1]An intertwiner is a map between representations of a group that commutes with the action of the group.

$(g_p = I)$ are assigned an amplitude of unity. We shall follow the common practice of discussing the phase structure of a lattice theory using the β parameter $\beta = \frac{4}{\gamma^2}$.

We now turn to the definition of the dual model for the specific case of $G = SU(2)$ pure Yang-Mills in three dimensions. Starting from the conventional formulation of the lattice partition function $\mathcal{Z}$ given in (4) above, the duality transformation can be applied (see Appendix A.1) to yield the following expression for $\mathcal{Z}$ in terms of the dual variables:

$$(7) \qquad \mathcal{Z} = \sum_j \left(\sum_i \prod_{v \in V} 18j^v(i_v, j_v) \prod_{e \in E} N^e(i_e, j_e)^{-1} \right) \left(\prod_{p \in P} e^{-\frac{2}{\beta} j_p(j_p + 1)}(2j_p + 1) \right).$$

Here V denotes the vertex set of the lattice, while the summations over i and j range over all possible edge and plaquette labellings, respectively. A plaquette labelling j assigns an irreducible representation of $SU(2)$ to each element of P. These representations are labelled by non-negative half-integers (we will denote this set by $\frac{1}{2}\mathbb{N}$) and are referred to as *spins*; a labelling j is thus a map $j\colon P \to \frac{1}{2}\mathbb{N}$. An edge labelling i, on the other hand, is valued in a basis of maps that intertwine the representations of the plaquettes incident on the same edge. In our present case, the choice of basis corresponds to a grouping of the four incident plaquette spins into two pairs. When such an edge splitting has been made, the intertwiners may also be labelled by spins, as described just before Definition 2.2 and in Appendix A.2. Different choices of splitting can be made, but, some are more computationally efficient than others. In writing (7), we assume a fixed choice of splitting has been made and so an edge labelling is a map $i\colon E \to \frac{1}{2}\mathbb{N}$.

In the first pair of parentheses of (7), there is a product of $18j$ *symbols*, each of which is a function of the 18 spins which label the 12 plaquettes and 6 edges incident to a vertex v; we denote the spins which appear by j_v and i_v. Next to it is a product of edge normalizations N^e depending on the edge spin i_e and on the four spins j_e labelling the plaquettes incident on e. It is important to recognize that the $18j$ symbol and the normalization factors N^e are purely representation-theoretic quantities (independent of the action chosen) and that, from a computational viewpoint, they represent the non-trivial part of the amplitude evaluation. Efficient algorithms can be found (using diagrammatic techniques similar to those used in [8]) for computing the $18j$ symbols and edge normalizations. Two of these are reviewed in Appendix A.2.

In the second parentheses of (7) there is a product of factors depending on j_p only; these arise from the character expansion coefficients of the heat kernel action (5) and are clearly straightforward to compute.

For the purposes of this paper, we define a *spin foam* to be an assignment of spins and intertwiners to the plaquettes and edges of the lattice[2], respectively. We define *supported spin foams* to be those with non-vanishing amplitude, and denote the set of them by $\mathcal{F}^+$. In terms of the supported spin foams we can write (7) as:

$$(8) \qquad \mathcal{Z} = \sum_{f \in \mathcal{F}^+} \mathcal{A}(f) = \sum_{f \in \mathcal{F}^+} \left(\prod_{v \in V} 18j^v(i_v, j_v) \prod_{e \in E} N^e(i_e, j_e)^{-1} \right) \left(\prod_{p \in P} e^{-\frac{2}{\beta} j_p(j_p + 1)}(2j_p + 1) \right).$$

It turns out that the spin foams that actually make a non-zero contribution to $\mathcal{Z}$ are highly constrained, a fact that is not manifest in (7) where every possible edge and plaquette coloring contributes a term. Moreover, once the plaquette spins have been specified, there is a limited range of intertwiner spins that give a non-zero amplitude. The details of these constraints will be discussed in Section 2.2.

The essential challenge for performing Metropolis simulations with this model is to find a set of moves that connect all the supported spin foams $\mathcal{F}^+$. To see why this is a non-trivial task, observe that if one has any supported spin foam and adds or removes a half-unit of spin from a single plaquette, the result will be a spin foam with vanishing amplitude; this follows immediately from the parity condition (see Definition 2.1 below), enforced by the $18j$ symbol. Changing single plaquettes by two half-units of spin preserves parity but restricts one to a single parity class. Thus a move involving a single plaquette is

---

[2]In spin foam quantum gravity, the 2-cells and 1-cells of a simplicial complex are typically used, rather than the plaquettes and edges of a cubic lattice. The general definition of spin foam was introduced by Baez in [4].

"too local" and so moves involving multiple plaquettes and edges simultaneously are needed. We now turn to this problem.

2.2. **Algorithm Construction — Ergodic Moves.** We first define the set of *admissible plaquette configurations*. These configurations are precisely those plaquette labellings that satisfy *edge admissibility* at every edge of the lattice:

Definition 2.1 (Edge admissibility)**.** The spins assigned to plaquettes incident to an edge are said to be *edge admissible* if the *parity* and *triangle inequality* conditions are satisfied. Writing j_1, j_2, j_3 and j_4 for the four spins incident to a given edge, these conditions are:

(1) **Parity**:
$$j_1 + j_2 + j_3 + j_4 \text{ is an integer.}$$
(2) **Triangle Inequality**: for each permutation (k, l, m, n) of $\{1, 2, 3, 4\}$ we have
$$j_k + j_l + j_m \geq j_n.$$

These conditions are equivalent to the existence of a non-zero invariant vector in the $SU(2)$ representation $j_1 \otimes j_2 \otimes j_3 \otimes j_4$.

If a splitting has been made for the edge, say with j_1 and j_2 on one side and j_3 and j_4 on the other, then the triangle inequality can be written in the less symmetric form

$$(9) \qquad |j_1 - j_2| \leq j_3 + j_4, \ |j_3 - j_4| \leq j_1 + j_2.$$

Representation-theoretically, the less symmetric form says that there exists a non-trivial intertwiner between $j_1 \otimes j_2$ and $j_3 \otimes j_4$. A basis of such intertwiners is labelled by spins which match parity with $j_1 + j_2$ and $j_3 + j_4$ and fall into the specific range defined below. This leads us to the following definition of an *admissible spin foam*:

Definition 2.2 (Admissible spin foam)**.** A spin foam is *admissible* if and only if:
(1) The assignment of spins to plaquettes is everywhere edge admissible.
(2) For every edge $e \in E$, i_e satisfies
$$i_e + j_1 + j_2 \text{ and } i_e + j_3 + j_4 \text{ are integers}$$
and
$$i_e \in I_e \equiv [|j_1 - j_2|, j_1 + j_2] \cap [|j_3 - j_4|, j_3 + j_4],$$
where $[a, b] \equiv \left\{ j \in \frac{1}{2}\mathbb{N} \mid a \leq j \leq b \right\}$.

We call the interval I_e the *range* of the triangle inequalities at edge e. It is guaranteed to be non-empty by edge admissibility. We denote the set of admissible spin foams by $\mathcal{F}^A$.

At this point we observe that while any supported spin foam is admissible, the converse does not necessarily hold, as the amplitude can vanish despite admissibility conditions being satisfied. We define *exceptional spin foams* to be admissible spin foams of vanishing amplitude and denote them by $\mathcal{F}^E \equiv \mathcal{F}^A \setminus \mathcal{F}^+$. In practice, exceptional spin foams are rarely encountered during simulation. If one assumes that exceptional spin foams are sufficiently isolated (i.e. do not form surfaces that separate the configuration space) then the question of ergodicity will not be affected, i.e. it will be sufficient to show ergodicity of moves on admissible spin foams. In what follows, we shall make this assumption and refer to it as the *isolation of exceptionals* hypothesis.

Before considering ergodicity with respect to spin foams, it is useful to first describe moves by which any admissible *plaquette* configuration can be reached from any other admissible plaquette configuration:

Definition 2.3 (Plaquette cube move)**.** A *plaquette cube move* consists of
(1) A choice of 3-cell of the cubic lattice. These are simply the smallest cubes of the lattice, with 6 plaquettes, 12 edges, and 8 vertices.
(2) For each of the 6 plaquettes of the 3-cell, a change is made to that spin by $+\frac{1}{2}$ or $-\frac{1}{2}$ units of spin.

It can be shown that these moves are ergodic on the space of admissible plaquette configurations (ignoring for the moment non-trivial global topology of the lattice[3]); a similar argument is used for instance in [5].

We next observe that, within our present context where the amplitude depends on intertwiner labellings, the plaquette cube moves will transform between *admissible* plaquette configurations but *inadmissible* spin foams, unless some simultaneous changes are made to the intertwiners labelling the edges of the cube. This leads us to define *spin foam* cube moves as follows:

Definition 2.4 (Spin foam cube move). A *spin foam cube move* consists of the following:

(1) A plaquette cube move.
(2) For each edge in the 3-cell chosen for the plaquette cube move, a randomly chosen change is made to the intertwiner labelling that edge, from a fixed set of possible changes. The possible changes are such that for any plaquette cube move, there is always a change that results in an admissible spin foam. The intertwiner changes that are proposed depend on how the edges are split within the selected cube; further details can be found in Appendix A.3.

We should mention here that for all the spin foam moves discussed in this section there will be many moves that are rejected immediately due to violation of the constraints; these are nonetheless counted as moves in order to satisfy detailed balance.

By construction, spin foam cube moves will reach some subset of intertwiner labellings for each plaquette configuration. The possibility that this may omit some admissible intertwiner configurations leads us to introduce an independent edge move.

Definition 2.5 (Spin foam edge move). A *spin foam edge move* consists of the following:

(1) An edge is selected.
(2) The intertwiner label is incremented or decremented by two half-units of spin (to preserve parity).

To see that the combination of spin foam cube and edge moves are ergodic on admissible spin foams (up to non-trivial global homology), we argue as follows. Observe that the spin foam cube moves allow us to move freely amongst the admissible plaquette configurations. To reach any given spin foam, one first obtains the associated plaquette configuration through the spin foam cube moves. We then apply whatever spin foam edge moves are needed to set the edge labels to their given values. This is possible because the admissible ranges I_e are connected by spin foam edge moves.

We now turn to the the issue of configurations arising from the non-trivial global topology of the lattice. It is common in lattice computations to impose periodic boundary conditions which are toroidal; i.e. in the present case the lattice is a discretization of the 3-torus. For these boundary conditions, if one introduces a sheet of half-unit spin having non-trivial global topology (see Figure 1, right), the spin foam cube moves are not able to remove it. Such a sheet (and its deformations by cube moves) can be introduced in any of the three directions of the 3-torus, in correspondence with the three generators of the second homology group of the 3-torus. A simple way to move between configurations corresponding to different homology classes is to create and remove sheets of half-unit spin; we do this by introducing the following moves:

Definition 2.6 (Spin foam homology move). A *spin foam homology move* consists of the following:

(1) A 2-dimensional plane of plaquettes spanning the lattice is selected. Applying periodic boundary conditions, this plane topologically defines a 2-torus wrapped around the 3-torus.
(2) For the selected plane, change each edge and plaquette label contained in it by the same amount, either $+\frac{1}{2}$ or $-\frac{1}{2}$.

We note that the cost of computing the change in amplitude induced by these moves scales with L^2 (where L is the side length of the lattice), making them costly for large lattices; we shall return to this point in our discussion below.

Now we have all the components to give a simple statement of our algorithm.

---

[3]If boundary conditions result in a lattice of non-trivial homology, homology changing moves must be added, as described below.

Algorithm 2.7. *(Ergodic spin foam algorithm)* A single iteration of the algorithm consists of the following:

(1) Apply a single spin foam cube move, spin foam edge move, or spin foam homology move.
(2) For the edges affected by the move, immediately reject the move if any spin foam admissibility condition is violated.
(3) Accept the move if $\frac{|A_{new}|}{|A_{old}|} > \alpha$, where A_{new} and A_{old} denote the spin foam amplitudes before and after the move, and α is a sample drawn from from the uniform distribution on the unit interval.

Step 1 gives a choice from among a set of moves that are ergodic on admissible spin foams, not just within a homology class but between classes as well. For each type of move, detailed balance is guaranteed as any move and its inverse is proposed with equal probability. The relative probability of proposing a cube, edge, or homology move can be freely chosen, for example to tune the algorithm for better convergence or acceptance rate. Step 2 could in principle be absorbed into Step 3, as the zeroes of the $18j$ symbols enforce all the admissibility constraints. In practice, admissibility is very easy to check and so one can often avoid computing the full $18j$ symbol. Step 3 is just the usual Metropolis acceptance condition; observables depending on the dual variables can be measured at each iteration or at regular intervals. The absolute value of the amplitudes in Step 3 are necessary due to the possibility of negative amplitudes (arising from the $18j$ symbols). The standard sign trick for computing expectation values in this situation is reviewed in Section 2.3.2.

In summary, we have defined a dual Metropolis algorithm for non-abelian $SU(2)$ pure Yang-Mills in the case of three dimensions. Assuming the isolation of exceptionals hypothesis, this algorithm is ergodic on supported spin foams. Before presenting results for our algorithm in Sections 3 and 4, we review some practical points of implementation.

2.3. Algorithm Construction — Practical considerations. When using the above algorithm, there are a number of novel considerations that don't apply to the conventional case. We discuss some of the more important ones here.

2.3.1. *Spin foam versus plaquette configuration simulation.* It is possible to define an alternative dual algorithm based upon plaquette configurations (rather than spin foams, which include intertwiner labels), using the plaquette cube moves to move ergodically between all admissible plaquette configurations. By applying the intertwiner expansion and fast evaluation of the $18j$ symbols, one can automate the computation of plaquette configuration amplitudes. This would proceed by writing the partition function (7) in terms of an intertwiner independent amplitude:

$$(10) \quad \mathcal{Z} = \sum_j \hat{A}(j), \quad \hat{A}(j) \equiv \left(\sum_i \prod_{v \in V} 18j^v(i_v, j_v) \prod_{e \in E} N^e(i_e, j_e)^{-1} \right) \left(\prod_{p \in P} e^{-\frac{2}{\beta} j_p(j_p+1)} (2j_p + 1) \right),$$

where the amplitude $\hat{A}(j)$ is a function of plaquette labelling j only; i.e. the full sum over intertwiner labels has been absorbed into the amplitude for a given plaquette labelling.

The question then becomes whether this algorithm is practical. We found that the answer depends crucially on the strength of the coupling. For comparison, we implemented the plaquette configuration simulation and were able to achieve good agreement with conventional results at *sufficiently strong coupling* ($\beta < 1.8$), where configurations involving large intertwiner sums are penalized by the amplitude. However, starting at $\beta \approx 1.8$ the simulation began to spend time in plaquette configurations with a large space of admissible intertwiner labellings; because the summations are nested there are a huge number of edge labelled terms being evaluated for a single plaquette configuration. Compounding this situation is a second critical drawback, in that for many configurations (and increasingly so at weaker coupling) the terms in the intertwiner summations couple edges that are arbitrarily distant in the lattice. Thus, at large lattice sizes and weak coupling the cost of computing the change in amplitude due to a single move will on average be of the order of the lattice volume.

The spin foam algorithm defined in Section 2.2 avoids both problems by making local changes to both plaquettes and edge labels. In summary, rather than importance sampling the plaquette configurations with a generally expensive, non-local amplitude (the intertwiner sum), one applies importance sampling

to the innermost terms of (7), which carry both plaquette and edge labels. While this involves a larger space of configurations, the evaluation of amplitudes proceeds extremely rapidly and independent of coupling. The observation that such a local algorithm exists for dual Yang-Mills theories (and also for dimensions higher than 3) was made by Halliday and Suranyi in [14], although they do not make explicit use of the spin foam formalism.

2.3.2. *Sign Problem.* Because the $18j$ symbol can take on negative values, the most straightforward form of the Metropolis algorithm is not applicable. Nonetheless, one can try to avoid this problem by applying what is commonly referred to as the "sign trick", e.g. [41]. We note that the sign trick was also employed in the work of Hari Dass [16]. Letting $\epsilon(f)$ denote the sign of the amplitude $A(f)$ for spin foam f, one can express the expectation value of an observable $O(f)$ as follows:

$$(11) \qquad \langle O \rangle = \frac{\sum_{f \in F^+} O(f) A(f)}{\sum_{f \in F^+} A(f)} = \frac{\sum_{f \in F^+} O(f) \epsilon(f) |A(f)|}{\sum_{f \in F^+} \epsilon(f) |A(f)|} = \frac{\left(\frac{\sum_{f \in F^+} O(f) \epsilon(f) |A(f)|}{\sum_{f \in F^+} |A(f)|} \right)}{\left(\frac{\sum_{f \in F^+} \epsilon(f) |A(f)|}{\sum_{f \in F^+} |A(f)|} \right)} = \frac{\langle \epsilon O \rangle_{||}}{\langle \epsilon \rangle_{||}}.$$

Observe that we now have a ratio of two expectation values, which can be estimated using simulations of a system governed by the *absolute value* $|A(f)|$ of the original amplitude (we indicate this by adding a subscript $||$). A common failing of this approach is that for many systems studied in quantum Monte Carlo (where the sign problem arises frequently), both numerator and denominator of the expression decay exponentially with a parameter under study. In such cases there are more sophisticated approaches available; invariably, resolving a serious sign problem requires exploiting foreknowledge of the distribution of positive and negative weights in the configuration space.

As discussed in Section 4, for the range of $\beta < 2.85$ and lattice sizes up to the maximum studied (16^3), the numerator and denominator of (11) are of order unity. In this regime, the sign problem is very tame and does not prevent accurate results from being obtained.

2.3.3. *Cost of Homology Moves.* Due to the extended nature of the structures added and removed by the homology moves (involving on the order of L^2 vertices and plaquettes), the associated change in amplitude becomes increasingly expensive to calculate for larger lattices. The situation for the present case of $SU(2)$ Yang-Mills in three dimensions can be summarized as follows. Homology changing moves are necessary to achieve agreement with conventional code on very small lattices, such as the 2^3 lattice discussed in Section 3. However, we have found in practice that as the lattice size increases, the frequency with which homology moves are attempted can be greatly decreased and ultimately set to zero without affecting the result. This is because adding a sheet of half-unit spin has a very low acceptance rate for larger lattices. We should mention however that for different spin foam models, particularly those which are in a deconfining phase, the non-trivial homology sectors of the ensemble will likely make significant contributions for arbitrarily large lattice sizes, and so cannot be neglected.

3. Verification of Dual Metropolis Code on a Small Lattice

Before proceeding to simulations at larger lattice size, an implementation of the dual algorithm described in Section 2 was verified on a 2^3 lattice. For this lattice and all lattices discussed in the paper, toroidal boundary conditions were applied. The observable measured was $\frac{1}{N} \sum_{p \in P} j_p$, the average spin per plaquette. The expectation value for this observable is:

$$(12) \qquad \langle j \rangle = \frac{\sum_{f \in \mathcal{F}} \left(\frac{1}{N} \sum_{p \in P} j_p \right) \mathcal{A}(f)}{\sum_{f \in \mathcal{F}} \mathcal{A}(f)}.$$

From the translation invariance of our lattice, this is a good estimator for the expectation value of spin on a single plaquette.

While too small to be of physical interest, the 2^3 lattice size makes it easy to check agreement between different Monte Carlo algorithms, as convergence is fast on smaller lattices. Moreover, by applying a spin cutoff it is possible to *exactly* compute the (cut-off) partition function of the dual model on a 2^3 lattice. This is done for cutoffs $j_{cut} = \frac{1}{2}$ and $j_{cut} = 1$, which correspond to the restrictions that $j \in \{0, \frac{1}{2}\}$ and $j \in \{0, \frac{1}{2}, 1\}$, respectively. While $j_{cut} = 1$ gives on the order of 10^{10} configurations on the 2^3 lattice, the case of $j_{cut} = \frac{3}{2}$ already requires on the order of 10^{15} configurations and is not
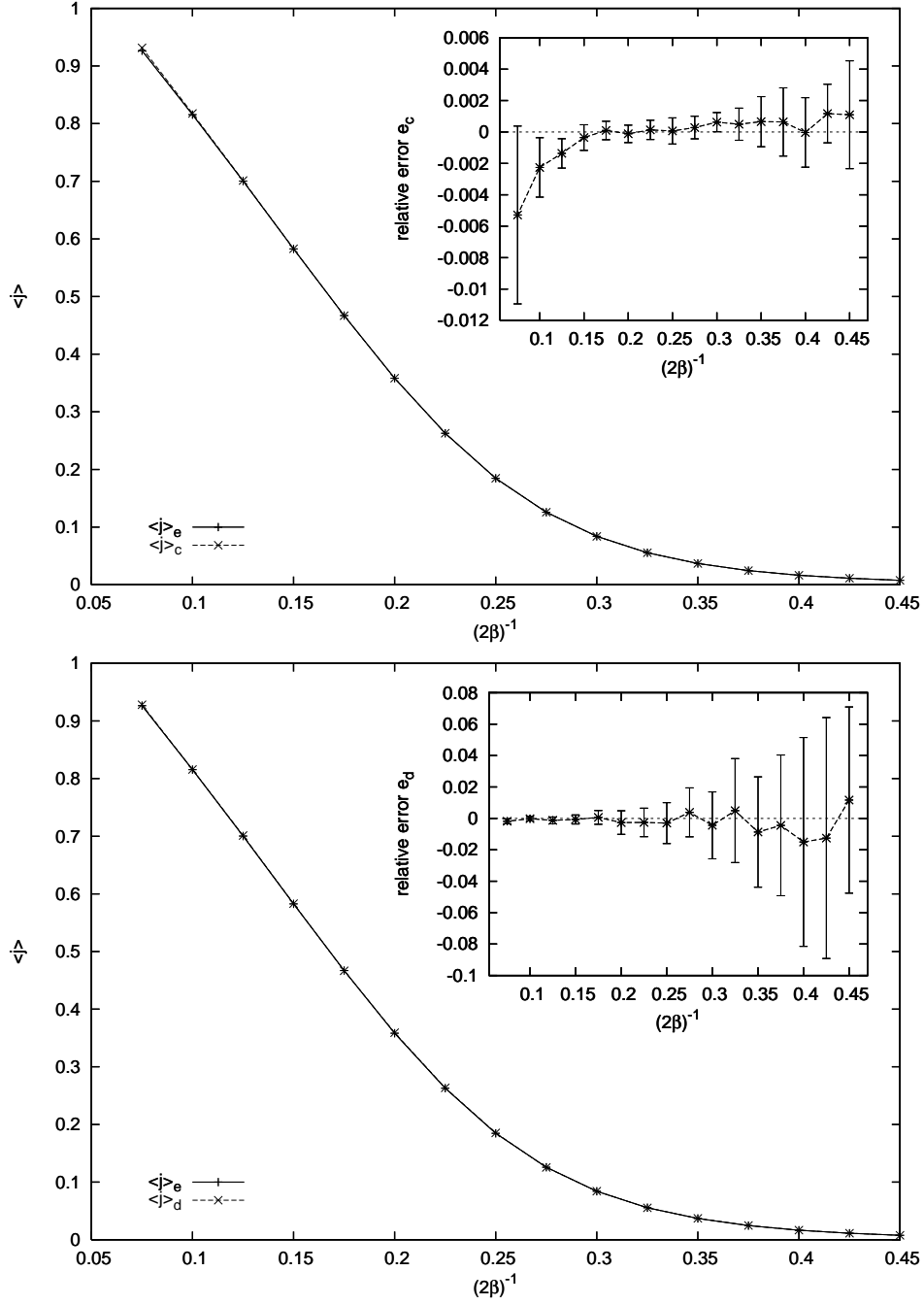
FIGURE 2. Comparison of conventional (top) and dual (bottom) computations with exact dual result on 2^3 lattice for $j_{cut} = 1$.

practical. In Figure 2, we show the results for spin cutoff $j_{cut} = 1$. For the conventional computations, the cut-off is realized by truncating the character expansion of the heat kernel; e.g. for $j_{cut} = 1$ only the first three terms of the character expansion are used. This truncation leads to a mild sign problem for the conventional calculation that can be resolved using the sign trick for the range of β presented here.
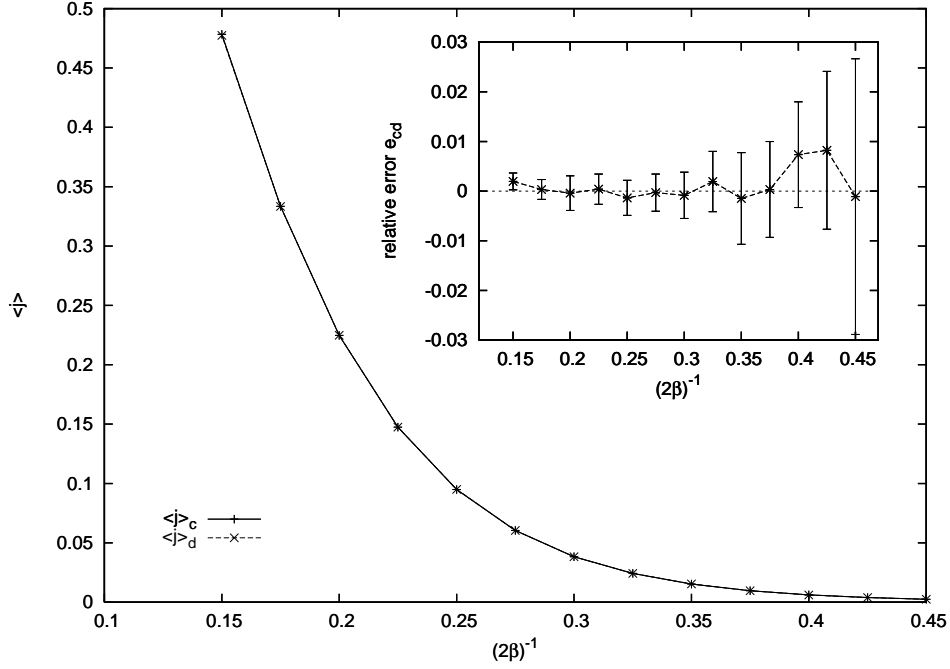
FIGURE 3. Conventional and dual results for the 8^3 lattice.

The main plots in Figure 2 each show two curves which appear on top of each other. The inset plots show the relative errors

$$(13) \qquad e_c \equiv \frac{\langle j \rangle_e - \langle j \rangle_c}{\langle j \rangle_e} \quad \text{and} \quad e_d \equiv \frac{\langle j \rangle_e - \langle j \rangle_d}{\langle j \rangle_e},$$

where the subscripts c, d and e refer to the conventional, dual and exact calculations. The expectation values $\langle j \rangle_c$ and $\langle j \rangle_d$ and their standard deviations were found from the results of 12 runs of 7.5×10^8 simulation steps each. The error bars are 3σ in magnitude. The data is consistent with the expected error being zero.

4. TESTING THE DUAL ALGORITHM

4.1. **Results.** In this section we describe results obtained on an 8^3 lattice over a range of coupling constants. For dual spin foam simulations, 25 runs of 10^{10} moves were used to generate the data shown in Figure 3; for the conventional results, 15 runs of 10^9 moves were used. The observable measured was the expectation value $\langle j \rangle$ of the spin observable, as described in Section 3. In the main part of Figure 3, the expectation value for both conventional and dual results are shown, with standard deviation computed from the results of different runs. Qualitatively, we see that the two algorithms are in very good agreement, as the curves fall nearly on top of one another. To better exhibit the detailed behavior, the inset plots show the relative error $e_{cd} \equiv \frac{\langle j \rangle_c - \langle j \rangle_d}{\langle j \rangle_c}$. The standard deviation in the relative error was computed by combining the standard deviations of the expectation values. All error bars are 3σ in magnitude. We find agreement between the two algorithms within about 1%, which is within the estimated error.

The results for lattices of size 4^3 and 16^3 are very similar. The above computations were done with the ladder recoupling of the $18j$ symbol (see Appendix A.2.1) due to its simpler implementation. For the range of coupling presented, we found that the results were insensitive to increases in the cut-off past $j_{cut} = 3$, which was the specific value used for both the dual and conventional data.

4.2. **Slow-down at weak coupling.** With the current implementation of the algorithm, there is a problem in obtaining results for $\beta \geq 2.85$. For these β, the Metropolis simulation eventually becomes "trapped" in a region of higher spin than untrapped configuations. These trapped regions appear to

have steep or narrow exits, as the simulation remains trapped for the duration of the computation. This behavior is also observed in some runs at stronger coupling (small β); the trapped mode generally takes a longer time to develop as coupling is increased, and is absent entirely from most of the runs at the strongest couplings considered.

While the precise nature of this slow-down is not yet fully understood, it shows some of the symptoms of similar problems noted for dual $U(1)$ in three dimensions. In [12], long autocorrelation times (not seen with the conventional code at the same β) are observed past a certain β. Slow-down of dual algorithms due to overly local moves at weak coupling is also alluded to in [44, 45, 46] for $U(1)$ in four dimensions.

By analogy with the existing literature on the dual $U(1)$ case, it is possible that the solution will involve adding moves that simultaneously change spins over regions that are larger than the minimal cube. A useful analog to consider may be spin systems, where the variables are also discrete and slow-down has been successfully addressed using cluster algorithms [27]. In our case, the presence of admissibility and parity constraints tends to make it difficult to find moves with reasonable acceptance rates. As is common with cluster algorithms, the "size" of the extended moves will likely need to be tuned with β.

5. Outlook for further Development

5.1. Generalizations.
Although we have so far limited ourselves to $SU(2)$ pure Yang-Mills in three dimensions, the algorithm we describe is in principle straightforward to extend to more physically relevant models.

5.1.1. *Wilson Loop Observables.*
The theory behind Wilson loop observables in the dual spin foam picture can be found in the work of [33]. The basic challenge for computations is the fact that, in the dual, the Wilson loop is a ratio of two partition functions with different admissibility conditions. In a forthcoming paper, we describe how to extend the method described here to define a Metropolis algorithm for Wilson loop observables [7].

5.1.2. *Four Dimensions.*
In four dimensions on a hyper-cubic lattice, the $18j$ symbol is replaced by its higher-dimensional analog[4], a $32j$ symbol (involving 24 plaquettes and 8 edges); for the heat kernel action the plaquette weights take the same form as in (7). As the edges will have six incident plaquettes, the triangle inequalities will be more involved. Assuming these differences can be accounted for, we expect an algorithm with the same general form will be feasible.

Of particular interest in $D = 4$ will be the behavior of autocorrelation times and simulation slow-down as the critical point (not present in three dimensions) is approached in the continuum limit of large lattice and weak coupling.

5.1.3. *Higher N Lie groups and their q-deformations.*
The algorithm has direct generalizations to $SU(3)$ and even $SU(N)$. Vertex amplitudes (generalizations of the $18j$ symbol) will likely be more intricate, as for higher N more than one discrete variable is needed to label a given irreducible representation. The basic structure of the algorithm in terms of moves on plaquette and intertwiner labels should go through, although admissibility constraints can be expected to take a more complicated form.

An interesting feature of the dual model is the ease with which q-deformed gauge groups $SU_q(N)$ can be treated once the infrastructure for computing with $SU(N)$ is in place. One illustration of this is recent work [9] where computations are performed with a q-deformed version of the Riemannian Barrett-Crane model of spin foam quantum gravity. In four dimensions, where one expects to approach a critical point in the continuum limit, it would be interesting to consider how computations of correlation functions are affected by q-deformation, for example whether or not distinct universality classes emerge.

---

[4]In the same way that the dual model [2] and [3] is equivalent to a particular recoupling of the $18j$ symbol (see Appendix A.2.2), we expect the $32j$ to agree with past work on dual forms of Yang-Mills in four dimensions [14].

5.1.4. *Other Extensions.* The above mentioned extensions of the method are straightforward. There are also intriguing (and more involved) possibilities of extending the method into the realm of dynamical fermions and to gravity. For incorporating dynamical fermions into a dual model, we are investigating an approach in which the polymer expansion of the fermion determinant plays a key role. For computing pure Yang-Mills coupled to spin foam quantum gravity, work by Oriti and Pfeiffer [35] provides a useful starting point. Developments in the theory of dual models [34, 39] indicate that the dual viewpoint has broad applications. We hope that concrete computational results will encourage its further development and offer an alternative means for analyzing theories of current interest.

6. Conclusions

Previous work with computing in the dual of non-abelian theories due to Hari Dass et al. [16, 17, 20] brought to light a number of important issues, but it had not been clear how these might be fully resolved.

The work reported here establishes that one can indeed obtain agreement with conventional lattice gauge theory using simulation with the dual form of the theory. Currently, the algorithm we describe has provided results on a 16^3 lattice for β up to 2.85, and work is underway to extend this to larger lattices and weaker coupling (higher β). We expect addressing higher β will involve introducing moves that change spin foams over a larger region of the lattice, as our algorithm appears to exhibit the symptoms of crossover to a delocalized, disordered phase as observed in [12, 44, 45, 46] for the case of dual three-dimensional $U(1)$. In four dimensions, the expectation is that similar behavior will be seen as the critical point is approached. The fact that cluster algorithms have been remarkably successful at addressing critical slow-down in discrete spin systems is promising in this regard and it is likely that some insights from this area may apply.

The ultimate impact of the sign problem is still not fully understood from the present work, as the sign expectation begins decreasing away from unity at close to the same β where the current simulation is obstructed by impractically long autocorrelation times. Assuming a practical resolution to the trapping problem can be found, it will be interesting to see whether or not the sign problem becomes a serious obstacle at weaker coupling.

An important property of our algorithm is the use of both plaquette labels and edge (intertwiner) labels as variables of the simulation. This allows the Metropolis algorithm to proceed through local moves whose changes in amplitude can be evaluated very rapidly. Using the spin foam formalism, ergodicity is fairly straightforward to show; it is essentially an extension of an algorithm used in previous (quantum gravity) spin foam computations [5, 9] to the case where intertwiner labels are changed as well. Our claim of ergodicity does however depend on the unproven hypothesis that exceptional zeros of the $18j$ symbol are isolated, i.e. the zeros do not form surfaces that separate the space of admissible spin foams. The agreement of our results with conventional computations can be viewed as evidence for this hypothesis.

Another interesting aspect of our algorithm is the necessity (for full ergodicity) of introducing moves that change homology class, in the case where boundary conditions lead to non-trivial global topology of the lattice. While for the specific model studied here such configurations have negligible weight for large lattices, in more general spin foam models (e.g. those in a deconfining phase) these configurations may play a more important role.

Also worth emphasizing is the important role of diagrammatic techniques in generating efficient algorithms for the $18j$ symbols. In particular, the formula of Anishetty et al. [2, 3] used in [16, 17, 20] can be derived very economically from a particular splitting of the $18j$ symbol, as we show in the Appendix.

While still in its very early stages (particularly in comparison with several decades development of conventional LGT codes), we believe dual computations have a promising future ahead. The algorithm we describe here immediately generalizes to higher N gauge groups and to four dimensions, and work is underway to incorporate dynamic fermions into the dual framework. The next major step is the computation of Wilson loop observables, currently in progress [7]. Finally, the application of the technique to spin-foam quantum gravity coupled to matter provides a long-term motivation for the present work.

Appendix A. The dual model, $18j$ symbol algorithms and compatible intertwiner moves

A.1. **Derivation of the dual model.** This section sketches some of the steps of the transformation from the conventional to the dual form of the lattice Yang-Mills partition function, (4) and (7) respectively. Our approach is inspired by the spin foam picture, and is closest to that found in [10]. Non-abelian dual models have also been analyzed from a spin foam perspective in [33, 34].

We begin by observing that, due to gauge invariance, the plaquette action $S(g_p)$ of (4) depends only on the conjugacy class of its argument. Thus, its exponential can be expanded in terms of group characters χ_j

$$e^{-S(g)} = \sum_j c_j \chi_j(g), \tag{14}$$

where j ranges over the equivalence classes of finite-dimensional irreducible unitary representations of the gauge group G. Substituting into (4) and interchanging the order of summation and integration yields

$$\mathcal{Z} = \sum_{\{j_p\}} \int \prod_{e \in E} dg_e \prod_{p \in P} c_{j_p} \chi_{j_p}(g_p). \tag{15}$$

At this point it is convenient to specialize to a $D = 3$ cubic lattice with periodic boundary conditions and to fix an orientation for the plaquettes and edges of the lattice. Choose a right-handed set of xyz axes for the lattice. Orient all of the edges in the positive coordinate directions. Every lattice cube is in the first octant of one of its vertices. Take each of the three plaquettes of the cube that are incident to this vertex and orient it in the counterclockwise direction, as seen from outside the cube. It is easy to see that this choice of orientations is translation invariant, that the orientation of each edge agrees with two of the four plaquettes incident on it and is opposite to the other two, and that every plaquette has two edges whose orientations agree with its own and two that do not.

With this choice of orientation, the holonomy around a plaquette p is $g_p = g_1 g_2 g_3^{-1} g_4^{-1}$, where g_1, g_2, g_3 and g_4 are the group elements associated to the edges of the plaquette p, starting with an appropriate edge and going cyclically. Recall that the inverse g_i^{-1} is used if the orientation of edge i does not agree with that of p. Thus

$$\chi_{j_p}(g_p) = U_{j_p}(g_1)_a^b \, U_{j_p}(g_2)_b^c \, U_{j_p}(g_3^{-1})_c^d \, U_{j_p}(g_4^{-1})_d^a, \tag{16}$$

where $U_j(g)_a^b$ denotes a matrix element with respect to a basis of the j representation. If we insert (16) into (15) and collect together factors depending on the group element g_e, we get a product of independent integrals over the group, each of the form

$$\int dg_e \, U_{j_1}(g_e)_{a_1}^{b_1} \, U_{j_2}(g_e)_{a_2}^{b_2} \, U_{j_3}(g_e^{-1})_{a_3}^{b_3} \, U_{j_4}(g_e^{-1})_{a_4}^{b_4} = \int dg_e \quad \begin{array}{c} \longleftarrow \bigcirc\!\!g_e \longleftarrow j_1 \\ \longleftarrow \bigcirc\!\!g_e \longleftarrow j_2 \\ \longrightarrow \bigcirc\!\!g_e^{-1} \longrightarrow j_3 \\ \longrightarrow \bigcirc\!\!g_e^{-1} \longrightarrow j_4 \end{array} \cdot \tag{17}$$

Here and below we use a graphical notation for tensor contractions, defined as follows. Each *wire* represents a matrix element of the unitary representation labelling it. Parallel wires represent products of such matrix elements. The four matrix elements in (17) come from the characters associated to the four plaquettes incident on the edge e. The free ends of the wires represent the indices of these matrix elements. The wires can be joined together into loops, one for each plaquette. The joining corresponds to contracting with other matrix elements from different edge integrals to form the product of characters as in (16).

Equation (17) defines a projection operator on the space of linear maps $j_4 \otimes j_3 \rightarrow j_1 \otimes j_2$. It is the usual group averaging operator whose image is precisely the intertwiners. Since it is a projection operator, it can be resolved into a sum over a basis of intertwiners $I_i : j_4 \otimes j_3 \rightarrow j_1 \otimes j_2$,

(18)

$$\int dg_e = \sum_i \frac{I_i I_i^*}{\langle I_i^*, I_i \rangle} = \sum_i \frac{}{},$$

where the intertwiners $I_i^* : j_1 \otimes j_2 \rightarrow j_4 \otimes j_3$ are chosen such that the trace $\langle I_{i'}^*, I_i \rangle$ of the composite $I_{i'}^* I_i$ is zero whenever $i' \neq i$ and non-zero if $i' = i$. The projection property is readily verified.

If, for each edge of the lattice, we fix a term i in the above summation, we can contract the intertwiners I_i and I_i^* with those coming from the other edges. At each vertex of the lattice, there will be six such intertwiners, and their contraction can be graphically represented as an octahedral network that we call the $18j$ symbol:

(19)

.

The vertices are labelled by the directions of the associated lattice edges emanating from the given lattice vertex, namely $\pm x$, $\pm y$, and $\pm z$. The value of the $18j$ symbol depends on the choice of basis elements I_i and $I_{i'}^*$ in (18), the six summation indices i labelling the edges, and the 12 incident plaquette labels j. Each normalization factor $N \equiv \langle I_i^*, I_i \rangle$ depends on the choice of basis elements at an edge, the summation index i on that edge, and the four plaquettes incident on that edge. Note that the choice of basis can be made independently at each edge.

The discussion up to this point has been quite general, assuming a 3-dimensional cubic lattice. Next, we specialize to $G = SU(2)$ and give the plaquette action character expansion coefficients. For the heat kernel (5), the expansion coefficients take the particularly simple form [30]

(20)
$$e^{-S(g)} = \frac{1}{K(I, \frac{\gamma^2}{2})} \sum_j (2j+1) e^{-\frac{\gamma^2}{2} j(j+1)} \chi_j(g), \quad j = 0, \tfrac{1}{2}, 1, \ldots,$$

where $K(g, t)$ is defined by (6). Putting these pieces together, we obtain the dual formula for the lattice Yang-Mills partition function

(21)
$$\mathcal{Z} = \sum_j \left(\sum_i \prod_{v \in V} 18j^v(j_v, i_v) \prod_{e \in E} N^e(i_e, j_e)^{-1} \right) \left(\prod_{p \in P} (2j_p + 1) e^{-\frac{\gamma^2}{2} j_p(j_p+1)} \right),$$

where an overall numerical factor of $K(I, \frac{\gamma^2}{2})$ per plaquette has been discarded. This precisely reproduces Equation (7), where we described the notation we are using for the plaquette and edge labellings j and i.

A.2. **Efficient algorithms for the** $18j$ **symbol via recoupling.** In order to perform computations with (21), we first need to choose explicit basis elements I_i and I_i^* of the spaces of intertwiners that appear in (18). Below, we consider two patterns for choosing such bases for each edge of the lattice, one we call the ladder recoupling and one we call the tetrahedral recoupling. They lead to different $18j$ symbols and have different properties with respect to lattice translations.

14

A.2.1. *The ladder recoupling.* Recall that for compatible spins j, k and m, there is an intertwiner $j \otimes k \to m$ that is unique up to scale. To be explicit, we choose the specific intertwiner defined in [6, 2.5.4], and we denote it by

(22)
$$
\begin{array}{c}
\vcenter{\hbox{\includegraphics{}}}
\end{array}
$$

Similarly, we use the same reference[5] to define

(23)

It is well-known that for fixed j_1, j_2, j_3 and j_4, the intertwiners

(24)
$$
I_i^v \equiv
$$

form a basis of the space of intertwiners $j_4 \otimes j_3 \to j_1 \otimes j_2$, as i varies over admissible spins. We call this the *vertical splitting*.

There is also a second vertical splitting, given by interchanging j_3 and j_4, which changes the intertwiner by a factor of $(-1)^{j_3+j_4-i}$. The geometry of the lattice provides a natural way to choose between the two: we make sure that the plaquette labels on the left (j_4 and j_1 above) are part of the same lattice cube, and same for the labels on the right.

A convenient choice of dual basis is given by

(25)
$$
I_i^{v*} \equiv
$$

One can check that $\langle I_{i'}^{v*}, I_i^v \rangle = 0$ for $i' \neq i$. We next need to evaluate the normalization factor

(26)
$$
N^v = \langle I_i^{v*}, I_i^v \rangle = i
$$

$$
i \, .
$$

In order to accomplish this, we now explain how to relate our tensor contraction diagrams to *spin networks*. While it would be possible to work entirely with tensor contraction diagrams, there are two reasons to switch to the spin network notation. First, spin networks do not require that the edges be directed, which relieves us of some complicated bookkeeping. Second, by using spin networks, we can take advantage of many existing formulas and software libraries for computing spin network evaluations.

Recall that a spin network is a trivalent undirected ribbon graph whose edges are labelled by spins. One assigns a value to a spin network in the following way. First, draw it in the plane, in general position, with the ribbon flat. Then, read it from top to bottom, interpreting the vertices as the trivalent intertwiners discussed above, and interpreting cups and caps as certain intertwiners which

---

[5]Note that our diagrams are read downwards, while those of [6] are read upwards.

can introduce signs. If the spin network is closed, the resulting intertwiner is a map from the trivial representation to itself, and so can be identified with a complex number. The result is independent of the embedding in the plane, a fact that is quite useful in computations. In particular, the trivalent intertwiners are chosen carefully so that the evaluation remains unchanged when inputs are deformed into outputs and vice versa. We refer the reader to [6] for more details. While the starting point is different, the formulas given in [24], with $A = 1$, also apply to these diagrams[6]. Note that some other authors have slightly different conventions, e.g. some take $A = -1$.

We will now work out how to compute tensor contractions using spin networks. Take a tensor contraction diagram involving just the trivalent intertwiners discussed above and draw it in the plane such that all edges are pointing downwards except for some edges which leave the bottom of the diagram and loop around to reenter at the top. If we erase the arrows, the resulting spin network will have the same interpretation as the tensor contraction diagram, except for the signs introduced in the cups and caps. One can show that the difference is exactly a factor of $(-1)^{2J}$, where J is the sum of the spins labelling the edges that loop around.

As a first example, the value of a loop labelled with j in the tensor notation is the dimension $2j+1$ of the representation. However, in the spin network notation, the value of a loop is $\Delta_j = (-1)^{2j}(2j+1)$.

Similarly, the value of the edge normalization factor is

$$(27) \qquad N^v = \langle I_i^{v*}, I_i^v \rangle = \;\;\boxed{\begin{array}{c} j_1 \;\; j_2 \\ i \\ j_4 \;\; j_3 \end{array}}\; i = (-1)^{2i}\;\boxed{\begin{array}{c} j_1 \;\; j_2 \\ i \\ j_4 \;\; j_3 \end{array}}\; i = (-1)^{2i}\frac{\theta(j_1, j_2, i)\,\theta(j_3, j_4, i)}{\Delta_i},$$

where $\theta(a, b, c)$ stands for the value of the following *theta network*:

$$(28) \qquad \theta(a, b, c) \equiv \;\;\begin{array}{c} a \\ b \\ c \end{array}.$$

Its value is given explicitly in [24, Chapter 9].

Note that the conversion sign factor $(-1)^{2i}$ from (27) can be expressed as $(-1)^{2(j_1+j_2)}$ by appealing to the parity constraints. Since each plaquette is "outgoing" from two edges, each plaquette spin contributes $(-1)^{4j} = 1$. In other words, the conversion sign factors from the edge normalizations N^v cancel. It can be shown that the conversion sign factor for the $18j$ symbol appearing in (19) is independent of the edge splitting and can be written as $(-1)^{2J}$, where, for instance, $J = j_{+x+y} + j_{+x-z} + j_{-y-z}$. Each plaquette spin shows up in exactly one such sign factor, so the signs combine to give $(-1)^{2J_{\text{tot}}}$, where J_{tot} is the sum of all plaquette spins. Note that on a lattice with two or more odd side-lengths, this sign factor can be non-trivial.

Next we must work out the value of the $18j$ symbols that arise using the vertical splitting. The corresponding spin network is obtained by applying this splitting to the vertices of the octahedron shown in (19) and erasing the arrows from its edges. A method for evaluating this spin network is shown in Figure 4. The calculation is similar to that of [8], where a "ladder" structure also appears. The recoupling move

$$(29) \qquad \begin{array}{c} b \qquad c \\ n \\ a \qquad d \end{array} \;=\; \sum_m \frac{\Delta_m \begin{bmatrix} a & b & m \\ c & d & n \end{bmatrix}}{\theta(a, d, m)\theta(b, c, m)} \;\begin{array}{c} b \qquad c \\ m \\ a \qquad d \end{array}$$

[6]Note that while we use half-integer spins, [24] uses twice-spins, which are always integers.

Vertex splitting

Redrawing in plane

Redrawing as a ladder (wrapped in a circle)

Recoupling to a bubble chain

$$\sum_m$$

$$\left[\begin{matrix} i_{+x} & j_{+x+y} & m \\ i_{-z} & j_{-y-z} & j_{+x-z} \end{matrix}\right] \left[\begin{matrix} j_{+x+y} & i_{+y} & m \\ j_{-x-z} & i_{-z} & j_{+y-z} \end{matrix}\right] \left[\begin{matrix} i_{+y} & j_{+y+z} & m \\ i_{-x} & j_{-x-z} & j_{-x+y} \end{matrix}\right]$$

$$\times \left[\begin{matrix} j_{+y+z} & i_{+z} & m \\ j_{-x-y} & i_{-x} & j_{-x+z} \end{matrix}\right] \left[\begin{matrix} i_{+z} & j_{+x+z} & m \\ i_{-y} & j_{-x-y} & j_{-y+z} \end{matrix}\right] \left[\begin{matrix} j_{+x+z} & i_{+x} & m \\ j_{-y-z} & i_{-y} & j_{+x-y} \end{matrix}\right] \left(\prod_{i=1}^{6} \frac{\Delta_m}{\theta(\cdots)\theta(\cdots)}\right)$$
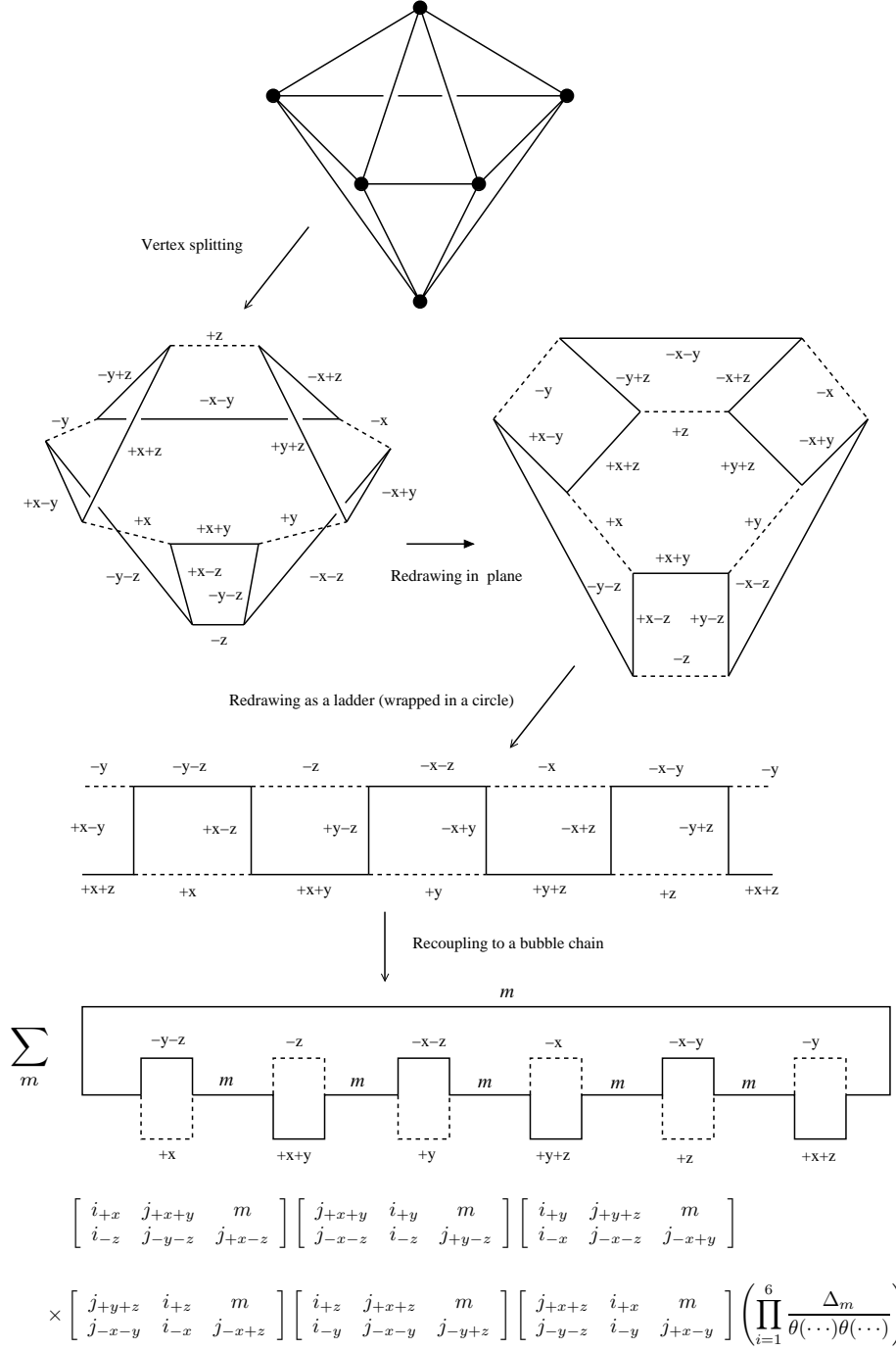
FIGURE 4. The ladder recoupling of the $18j$ symbol; a single sum.

is applied to each of the six "rungs" of the ladder, producing a chain of bubbles. The function of six spin labels appearing in (29) is the tetrahedral network, shown in the last step of Figure 5. The value of the tetrahedral network is given explicitly in [24, Chapter 9] and is closely related to the Wigner-Racah $6j$ symbol of angular momentum theory [31, Appendix B], see (31).

Because of Schur's Lemma, the six independent sums from the recoupling moves become a single sum. The bubbles are proportional to the identity, weighted by a theta network divided by a loop. Six theta networks arising from the bubbles cancel against six of the twelve theta networks from the

recoupling moves to give the six theta networks shown in the final line. The bubbles also contribute six loop factors (Δ_i) in the denominator, which exactly cancel the loop factors from the recoupling. The final result can be written as:

$$
(30) \quad \sum_m \frac{\Delta_m \displaystyle\prod_{6 \text{ bubbles}} \begin{bmatrix} \cdots & \cdots & m \\ \cdots & \cdots & \cdots \end{bmatrix}}{\theta(m,i_{+x},j_{-y-z})\,\theta(m,i_{-x},j_{+y+z})\,\theta(m,i_{+y},j_{-x-z})\,\theta(m,i_{-y},j_{+x+z})\,\theta(m,i_{+z},j_{-x-y})\,\theta(m,i_{-z},j_{+x+y})},
$$

where the arguments of the six tetrahedral networks are those that appear in the last line of Figure 4. The explicit relation between the tetrahedral network and the Wigner-Racah $6j$ symbols is

$$
(31) \quad \begin{bmatrix} J_1 & J_2 & J_3 \\ j_1 & j_2 & j_3 \end{bmatrix} = \sqrt{|\theta(J_1,J_2,j_3)\theta(j_1,j_2,j_3)\theta(J_1,j_2,J_3)\theta(j_1,J_2,J_3)|} \begin{Bmatrix} j_1 & j_2 & j_3 \\ J_1 & J_2 & J_3 \end{Bmatrix}.
$$

Note the row swap and the fact that the four theta networks correspond to the four triples of spins from the $6j$'s arguments that must satisfy triangle inequalities. For reference, $|\theta(a,b,c)| = (-1)^{a+b+c}\theta(a,b,c)$.

The $18j$ symbol described in this section was used in computing the data appearing in Sections 3 and 4.

A.2.2. *The tetrahedral recoupling.* Next we consider a different splitting of the vertices of the octahedron, which we call the tetrahedral recoupling. The $18j$ symbol that arises here is more efficient to compute than the $18j$ symbol for the ladder recoupling, because it does not require a sum. However, the splitting is not translation invariant, which makes it slightly harder to work with. This section is not needed in the rest of the paper, but is useful as a comparison to other sources and will be important for future calculations.

We begin by considering a different basis for the space of intertwiners $j_4 \otimes j_3 \to j_1 \otimes j_2$. It is given by the *horizontal splitting*

$$
(32) \qquad I_i^h \equiv
$$

as i varies over admissible spins. Note that it makes no difference which way the arrow on the edge labelled by i points.

There is also a second horizontal splitting, given by interchanging j_3 and j_4. As we did for the vertical splitting, we choose between the two by requiring that j_4 and j_1 label plaquettes that are part of the same cube. Unlike the vertical splitting, the two horizontal splittings are not in general related by a sign.

A convenient dual basis is given by

$$
(33) \qquad I_i^{h*} \equiv
$$

The traces $\langle I_{i'}^{h*}, I_i^h \rangle$ work out to be

$$
(34) \qquad N^h = \langle I_{i'}^{h*}, I_i^h \rangle = (-1)^{2(j_1+j_2)} \frac{\theta(j_1,j_4,i)\,\theta(j_2,j_3,i)}{\Delta_i}.
$$

For the tetrahedral recoupling, we use the vertical splitting (24) on three edges and the horizontal splitting on the opposite edges. The pattern we use is indicated in the first step of Figure 5. The result is a planar network consisting of four triangles connected to one another in a tetrahedral pattern.

For this recoupling, a minor complication arises because the intertwiner splittings are different on opposite edges. This means that a simple translation of the given tetrahedral $18j$ symbol to neighboring

Vertex Splitting

Redrawing in plane

Collapse Triangles

$$\frac{\left[\begin{array}{ccc} i_{+x} & j_{+x+z} & i_{+z} \\ j_{+y+z} & i_{+y} & j_{+x+y} \end{array}\right]}{\theta(i_{+x},i_{+y},i_{+z})} \frac{\left[\begin{array}{ccc} i_{+z} & j_{-y+z} & i_{-y} \\ j_{-x-y} & i_{-x} & j_{-x+z} \end{array}\right]}{\theta(i_{+z},i_{-x},i_{-y})}$$

$$\times \frac{\left[\begin{array}{ccc} i_{+x} & j_{+x-z} & i_{-z} \\ j_{-y-z} & i_{-y} & j_{+x-y} \end{array}\right]}{\theta(i_{+x},i_{-y},i_{-z})} \frac{\left[\begin{array}{ccc} i_{+y} & j_{-x+y} & i_{-x} \\ j_{-x-z} & i_{-z} & j_{+y-z} \end{array}\right]}{\theta(i_{+y},i_{-z},i_{-x})}$$
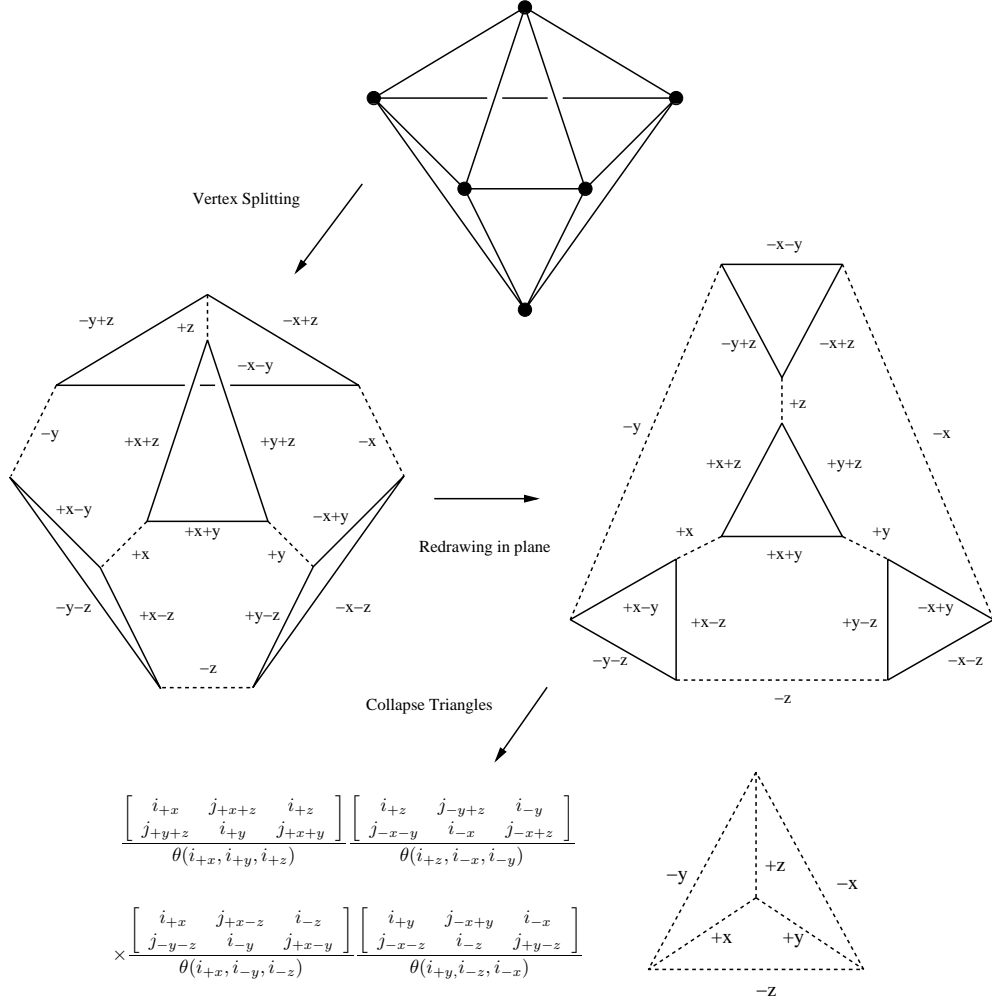
FIGURE 5. The tetrahedral recoupling of the $18j$ symbol; no sum.

vertices does not correspond to a consistent choice of basis for the intertwiners. This is easily overcome by dividing the lattice into a checkerboard of odd and even sites, and alternately using the original and reflected versions of the $18j$ symbol. For periodic boundary conditions, this does limit one to lattices with even side-lengths, but this constraint is not serious in practice.

As was the case with the ladder recoupling, the conversion sign factors from the normalization factors cancel, and the conversion sign factors from the $18j$ symbols give a factor of $(-1)^{2J_{\text{tot}}}$. In this case, because the checkerboard pattern forces even side-lengths, one can show that $(-1)^{2J_{\text{tot}}} = 1$.

The diagrammatic relation

(35)
$$\vcenter{\hbox{diagram}} = \frac{\left[\begin{array}{ccc} i_1 & j_2 & i_3 \\ j_1 & i_2 & j_3 \end{array}\right]}{\theta(i_1,i_2,i_3)} \vcenter{\hbox{diagram}}$$

can be used to collapse each of the four triangles into 3-valent vertices, as shown in the last step of Figure 5. The final result is simply:
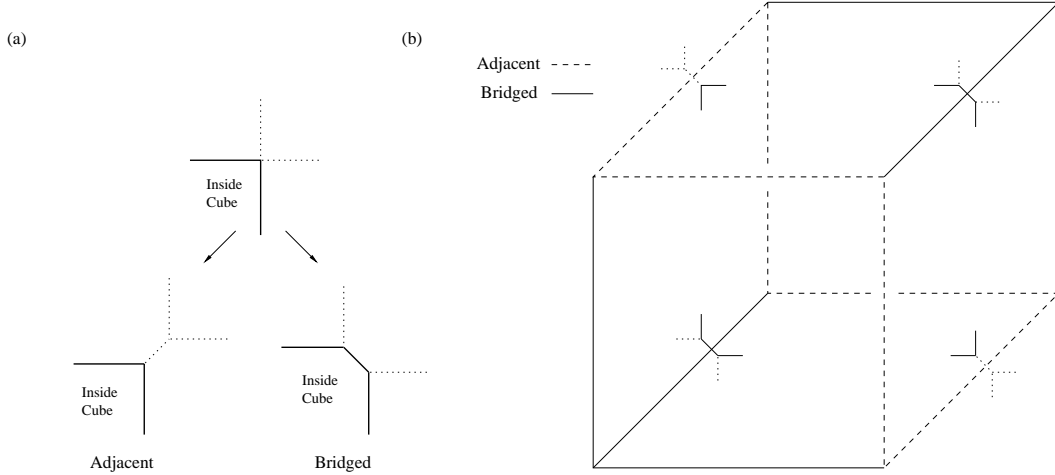
19

FIGURE 6. (a) The two types of splitting for an edge in a cube (side view). (b) Two possible splittings associated with the ladder recoupling for the edges of a cube.

$$(36) \quad \frac{\begin{bmatrix} i_{+x} & j_{+x+z} & i_{+z} \\ j_{+y+z} & i_{+y} & j_{+x+y} \end{bmatrix}\begin{bmatrix} i_{+z} & j_{-y+z} & i_{-y} \\ j_{-x-y} & i_{-x} & j_{-x+z} \end{bmatrix}\begin{bmatrix} i_{+x} & j_{+x-z} & i_{-z} \\ j_{-y-z} & i_{-y} & j_{+x-y} \end{bmatrix}\begin{bmatrix} i_{+y} & j_{-x+y} & i_{-x} \\ j_{-x-z} & i_{-z} & j_{+y-z} \end{bmatrix}\begin{bmatrix} i_{-x} & i_{-y} & i_{-z} \\ i_{+x} & i_{+y} & i_{+z} \end{bmatrix}}{\theta(i_{+x}, i_{+y}, i_{+z})\, \theta(i_{+z}, i_{-x}, i_{-y})\, \theta(i_{+x}, i_{-y}, i_{-z})\, \theta(i_{+y}, i_{-z}, i_{-x})}$$

Because this formula is essentially a product of tetrahedral networks with no auxiliary summations, it is highly efficient to compute.

The tetrahedral recoupling is easy to express in terms of Wigner-Racah $6j$ symbols using relation (31). In order to compare our work to other work, we give some of the details. Ignoring signs for the moment, the theta networks from the edge normalizations (27) and (34), the conversion formula (31), and the vertex amplitude (36) all cancel. Now we collect the signs of the theta networks. The theta networks from the edge normalizations contribute a sign of $(-1)^{2i}(-1)^{j_1+j_2+j_3+j_4}$, where i labels the edge and the j_k label the incident plaquettes. Since each plaquette is shared by four edges, the factors $(-1)^{j_1+j_2+j_3+j_4}$ cancel. Thus the edge normalizations become $(-1)^{2i}/\Delta_i = 1/(2i+1)$. Since this is positive, we can multiply each vertex amplitude by $\sqrt{2i+1}$ to take this into account. The theta networks from (36) contribute a sign of $(-1)^{\sum_{k=1}^{6} 2i_k}$, where the i_k label the edges incident on the vertex. Since each edge is shared by two vertices, the vertex signs also cancel. The final answer is that the vertex amplitude (36) becomes a product of five Wigner-Racah $6j$ symbols multiplied by a product of six factors of the form $\sqrt{2i+1}$.

We observe that in this form the tetrahedral recoupling is equivalent to the dual amplitude formula first proposed by Anishetty et al. [2, 3] and later used by Diakonov and Petrov [13]. The same formula was used in the computational work of Dass [16, 17, 20]. It should be emphasized that previous derivations of this formula did not make use of the spin foam formalism. As such, the identification of extra labels (those not coming from original plaquettes) with intertwiners was not explicit. We found this distinction between plaquette and intertwiner labels to be a crucial one in constructing our algorithm.

A.3. **Compatible intertwiner moves.** As mentioned in Definition 2.4, when a (single) spin foam cube move is applied, the 12 intertwiner labels of the selected cube have to be adjusted to ensure the result is an admissible spin foam. In general, admissible intertwiner changes depend on plaquette and edge labels of the cube. However, we will show next that this dependence takes on a simple form determined by the edge splittings.

For this discussion, we consider the case where the edges are split according to the ladder recoupling of the $18j$ symbol (see Figure 4), as the translation invariance of this recoupling simplifies the analysis. From the point of view of a cube move, edge splittings come in two kinds, see Figure 6(a). In one case, octahedral edges corresponding to adjacent cube plaquettes remain *adjacent* after the intertwiner

edge is introduced (type A). In the other, octahedral edges corresponding to adjacent cube plaquettes become *bridged* by the new intertwiner edge (type B). The pattern of type A and type B edges for a cube is shown in Figure 6(b).

The main constraint on the admissibility of intertwiner changes is parity, cf. Definition 2.2. For type A splittings, the two adjacent plaquette spins change by $\pm\frac{1}{2}$, forcing the corresponding intertwiner label to change by an integer. For type B splittings, the intertwiner, now bridging the two adjacent plaquettes, must change by a half-integer instead. A minimal set of admissible intertwiner changes now consists of 1, 0 or -1, for a type A edge, and $\frac{1}{2}$ or $-\frac{1}{2}$, for a type B edge. Note that negative and positive changes should be proposed with equal probability, to satisfy detailed balance.

In summary a *spin foam cube move* consists of the following:

(1) Choose a cube in the lattice.
(2) For each plaquette in the cube, adjust the spin independently by $+\frac{1}{2}$ or $-\frac{1}{2}$.
(3) For each type A edge in the cube, adjust the spin independently by 1, 0 or -1.
(4) For each type B edge in the cube, adjust the spin independently by $+\frac{1}{2}$ or $-\frac{1}{2}$.

References

[1] R. Anishetty, H. S. Sharatchandra. "Duality transformation for non-Abelian lattice gauge theories" (1990), *Phys. Rev. Lett.* **65**, Issue 7, 813–815.

[2] R. Anishetty, G.H. Gadiyar, M. Mathur, H.S. Sharatchandra. "Color invariant additive fluxes for SU(3) gauge theory" (1991), *Phys. Lett. B* **271**, 391–394.

[3] R. Anishetty, S. Cheluvaraja, H.S. Sharatchandra, M. Mathur. "Dual of 3-dimensional pure SU(2) Lattice Gauge Theory and the Ponzano-Regge Model" (1993), *Phys. Lett. B* **314**, 387–390.

[4] J.C. Baez. "Spin Foam models" (1998), *Class. Quant. Grav.* **15**, 1827–1858.

[5] J.C. Baez, J.D. Christensen, T. Halford and D.C. Tsang. "Spin foam models of Riemannian quantum gravity" (2002), *Class. Quant. Grav.* **19**, 4627–4648.

[6] J.S. Carter, D.E. Flath, M. Saito. *The Classical and Quantum 6j-Symbols.* (1995), Mathematical Notes 43, Princeton University Press, New Jersey.

[7] J.W. Cherrington. "Dual Computations for Non-Abelian Yang-Mills: Wilson Loop Observables". In preparation.

[8] J.D. Christensen, G. Egan. "An efficient algorithm for the Riemannian 10j symbols" (2002), *Class. Quant. Grav.* **19**, 1185–1194.

[9] J.D. Christensen, I. Khavkine. "q-deformed spin foam models of quantum gravity" (2007), *Class. Quant. Grav.* **24**, 3271–3290.

[10] F. Conrady. "Geometric spin foams, Yang-Mills theory, and background-independent models" (2005), arXiv:gr-qc/0504059v2.

[11] F. Conrady. "Analytic derivation of dual gluons and monopoles from $SU(2)$ lattice Yang-Mills theory. II. Spin Foam Representation" (2006), arXiv:hep-th/0610237v3.

[12] P.K. Coyle, I.G. Halliday, P. Suranyi. "$U(1)$ Lattice Gauge theory and its Dual" (1996), arXiv:hep-lat/9610031.

[13] D. Diakonov, V. Petrov. "Yang-Mills theory in Three Dimensions as Quantum Gravity Theory" (2000), J. Exp. Theor. Phys. **91**, 873–893; *Zh. Eksp. Teor. Fiz.* **91**, 1012–1035.

[14] I. Halliday, P. Suranyi. "Duals of nonabelian gauge theories in D dimensions" (1995), *Phys. Lett. B* **350**, 189–196.

[15] N.D. Hari Dass "On the analytical evaluation of the partition function of a unit hypercube in four dimensions"(1984), NIKHEF 12/84.

[16] N.D. Hari Dass. "Numerical Simulations of $D = 3$ $SU(2)$ LGT in the Dual Formulation" (2000), *Nuclear Phys. B Proc. Suppl.* **83**, 950–952.

[17] N.D. Hari Dass. "Quasi-local Update Algorithms for Numerical Simulations of d=3 $SU(2)$ LGT in the Dual Formulation" (2001), *Nuclear Phys. B Proc. Suppl.* **94**, 665–669.

[18] N.D. Hari Dass, P.G. Lauwers. "On the details of the variational investigations of $SU(2)$ Euclidean Lattice Gauge Theories"(1984), *Nucl. Phys. B* **235**, 535–562.

[19] N.D. Hari Dass, P.G. Lauwers, A. Patkos. "Variational Investigations of Euclidean $SU(2)$ Lattice Gauge Theories" (1983), *Phys. Lett. B* **130**, 292–296.

[20] N.D. Hari Dass, D. Shin. "Current Status of the Numerical Simulations of d=3 SU(2) LGT in the Dual Formulation" (2001), *Nucl. Phys. B Proc. Suppl.* **94**, 670–674.

[21] D. Horn, C.K. Zachos. "Lattice Action Forms Stable Under Renormalization" (1984), *Phys. Rev. D* **29**, 1202–1206.

[22] C. Itzykson, J. Drouffe. *Statistical Field Theory* (1989), Cambridge University Press, Cambridge.

[23] J. Jersak, T. Neuhaus, H. Pfeiffer. "Scaling analysis of the magnetic monopole mass and condensate in the pure $U(1)$ lattice gauge theory" (1999), *Phys. Rev. D* **60**, 054502.

[24] L. Kauffman, S. Lins. *Temperley-Lieb Recoupling Theory and Invariants of 3-Manifolds* (1994), Annals of Mathematics Studies, No. 134. Princeton University Press, New Jersey.

[25] J.B. Kogut. "The lattice gauge theory approach to quantum chromodynamics" (1983), *Rev. Mod. Phys.* **55**, 775–836.

[26] J.B. Kogut, M.A. Stephanov. *The Phases of Quantum Chromodynamics: From Confinement to Extreme Environments* (2004), Cambridge University Press, Cambridge.

[27] D.P. Landau, K. Binder. *A Guide to Monte Carlo Simulations in Statistical Physics* (2000), Cambridge University Press, Cambridge.

[28] C.B. Lang, C. Rebbi, P. Salomonson, B.S. Skagerstam. "The Transition from Strong Coupling to Weak Coupling in the SU(2) Lattice Gauge Theory" (1981), *Phys. Lett. B* **101**, Issue 3, 173–179.

[29] C.B. Lang, C. Rebbi, P. Salomonson, B.-S. Skagerstam. "Definitions of the gauge-theory coupling in lattice and continuum quantum chromodynamics: Implications of change in the lattice action" (1982), *Phys. Rev. D* **26**, 2028–2037.

[30] P. Menotti, E. Onofri. "The action of SU(N) lattice gauge theory in terms of the heat kernel on the group manifold" (1981), *Nucl. Phys. B* **190**, 288–300.

[31] A. Messiah. *Quantum Mechanics, Vol. 2* (1962), North-Holland, Amsterdam.

[32] I. Montvay, G. Munster. *Quantum Fields on a Lattice* (1994), Cambridge University Press, Cambridge.

[33] R. Oeckl, H. Pfeiffer. "The dual of pure non-Abelian lattice gauge theory as a spin foam model" (2001), *Nucl. Phys. B* **598**, 400–426.

[34] R. Oeckl. *Discrete Gauge Theory: From Lattices to TQFT* (2005), Imperial College Press, London.

[35] D. Oriti, H. Pfeiffer. "Spin foam model for pure gauge theory coupled to quantum gravity" (2002), *Phys. Rev. D.* **66**, 124010.

[36] K. Osterwalder, E. Seiler. "Gauge Field Theories on a Lattice" (1978), *Annals of Physics* **110**, 440–471.

[37] M. Panero. "A numerical study of a confined Q anti-Q system in compact $U(1)$ lattice gauge theory in 4D" (2004), Nucl. Phys. Proc. Suppl. **140**, 665–667.

[38] M. Panero. "A numerical study of confinement in compact QED" (2005), JHEP **05**, 066.

[39] H. Pfeiffer. "Exact duality transformations for sigma models and gauge theories" (2003), *J. Math. Phys.*, **44**, 2891–2938.

[40] L. Polley, U.-J. Wiese. "Monopole Condensate and Monopole Mass in $U(1)$ Lattice Gauge Theory" (1990), *Nucl. Phys. B* **356**, 629–654.

[41] H.D. Raedt, A. Lagendijk. "Monte Carlo Calculation of the Thermodynamic Properties of a Quantum Model: A One-Dimensional Fermion Lattice Model" (1981), *Phys. Rev. Lett.* **46**, 77–80.

[42] R. Savit. "Duality in field theory and statistical systems" (1980), *Rev. Mod. Phys.* **52**, 453–487.

[43] K.G. Wilson. "Confinement of Quarks" (1974), *Phys. Rev. D* **10**, 2445–2459.

[44] M. Zach, M. Faber, P. Skala. "Field Strength and Monopoles in Dual $U(1)$ Lattice Gauge Theory" (1997), *Nuclear Phys. B Proc. Suppl.* **53**, 521–523.

[45] M. Zach, M. Faber, P. Skala. "Flux tubes and their interaction in $U(1)$ lattice gauge theory" (1998), *Nucl. Phys. B* **529**, 505–522, arXiv:hep-lat/9709017v1.

[46] M. Zach, M. Faber, P. Skala. "Investigating confinement in dually transformed $U(1)$ lattice gauge" (1998), *Phys. Rev. D* **57**, 123–131.